Editors' Suggestion

Spin-Polarized Scanning Tunneling Microscopy Measurements of an Anderson Impurity

Mahasweta Bagchi,[1] Tfyeche Y. Tounsi,[1] Affan Safeer,[1] Camiel van Efferen,[1] Achim Rosch,[2] Thomas Michely,[1] Wouter Jolie,[1] Theo A. Costi,[3] and Jeison Fischer[1,*]

[1]*II. Physikalisches Institut, Universität zu Köln, Zülpicher Straße 77, 50937 Cologne, Germany*
[2]*Institut für Theoretische Physik, Universität zu Köln, Zülpicher Straße 77, 50937 Cologne, Germany*
[3]*Peter Grünberg Institut, Forschungszentrum Jülich, 52425 Jülich, Germany*

(Received 6 July 2024; revised 5 September 2024; accepted 6 November 2024; published 9 December 2024)

We report spin-polarized scanning tunneling microscopy measurements of an Anderson impurity system in MoS_2 mirror-twin boundaries, where both the quantum-confined impurity state and the Kondo resonance resulting from the interaction with the substrate are accessible. Using a spin-polarized tip, we observe magnetic-field-induced changes in the peak heights of the Anderson impurity states as well as in the magnetic-field-split Kondo resonance. Quantitative comparison with numerical renormalization group calculations provides evidence of the notable spin polarization of the spin-resolved impurity spectral function under the influence of a magnetic field. Moreover, we extract the field and temperature dependence of the impurity magnetization from the differential conductance measurements and demonstrate that this exhibits the universality and asymptotic freedom of the $S = 1/2$ Kondo effect. This work shows that mirror-twin boundaries can be used as a testing ground for theoretical predictions on quantum impurity models.

DOI: 10.1103/PhysRevLett.133.246701

The Kondo effect represents a paradigmatic example where many-body correlations play a pivotal role in its manifestation [1]. The microscopic origin of this phenomenon is rooted in the Anderson impurity model [2], which was originally introduced to describe how magnetic moments form in correlated impurity states that hybridize with a sea of conduction electrons. In the Kondo effect, these magnetic moments are gradually screened by the surrounding conduction electrons upon decreasing temperature. While the effect is conceptually straightforward, the theoretical framework to quantitatively describe it is demanding, requiring techniques such as the numerical renormalization group (NRG) [3,4] or the Bethe ansatz [5–7].

On the experimental front, scanning tunneling microscopy (STM) and spectroscopy (STS) techniques have stimulated new research on the Kondo effect over the last 25 years [8–15]. STM studies typically involve magnetic adsorbates on metallic surfaces [16]. Identification of the Kondo effect in spin-averaged STS often relies on measuring a Kondo zero-bias resonance (ZBR) [17], requiring temperature and field dependence to reduce the ambiguity of the assignment [18–21]. However, an unambiguous identification of the Kondo effect would ideally require measuring both the Kondo ZBR and the impurity peaks that give rise to the Kondo effect. For adsorbates on metallic surfaces, access to impurity levels has been elusive, due to the dominant presence of substrate states and their strong hybridization to the impurity states. This drawback impedes the exploration of the close connection between the Anderson and Kondo Hamiltonians as established by the Schrieffer-Wolff transformation [22]. It prevents, for example, identification of the large spectral weight rearrangements predicted for the spin-resolved spectral functions of an Anderson impurity in the presence of a magnetic field, even when the latter exceeds the thermal energy [23,24] (see Fig. 1). Previous spin-polarized STM measurements on adsorbates have demonstrated the spin polarization of the split Kondo ZBR [25–28], as expected from theory [29]. However, corresponding measurements of the Anderson model impurity peaks, where most of the spectral weight rearrangement occurs, have been absent.

In this Letter, we present spin-resolved STM measurements on MoS_2 mirror-twin boundaries (MTBs), where an Anderson impurity model is realized in a discrete half-filled quantum-confined state, for which both the impurity peaks and the Kondo resonance could be measured [30]. With spin-polarized STS, we detect changes in peak intensity of the quantum-confined impurity states with varying magnetic field, mirroring the changes seen in the split Kondo resonance. It demonstrates the field-dependent spectral weight rearrangement in the spin-resolved spectral functions in quantitative agreement with NRG simulations. By extracting field and temperature dependence of the impurity magnetization from the differential conductance, we demonstrate the universality and asymptotic freedom expected for an $S = 1/2$ Kondo system. Asymptotic

*Contact author: jfischer@ph2.uni-koeln.de

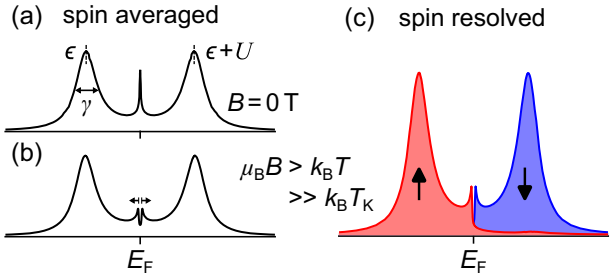

FIG. 1. Influence of a magnetic field on the spectral function of a magnetic impurity. Sketches based on NRG simulation ($\epsilon = -20$ meV, $U = 40$ meV, $\gamma = 9.0$ meV). (a) At 0 T, both spin components are equally distributed below and above the E_F, resulting in an unpolarized state. An external field ($g\mu_B B$, with $g = 2.5$) splits the Kondo resonance (marked by arrows) in the spin-averaged case (b) and induces a massive reorganization of the spectral distribution of the two spin components in the spin-resolved case (c).

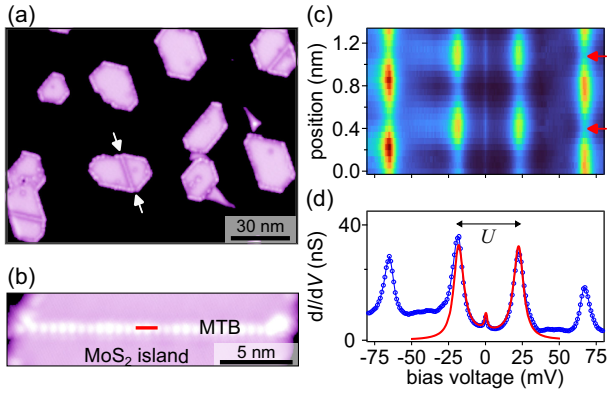

FIG. 2. Anderson impurity model in MoS_2 MTBs. (a) STM overview image of single-layer MoS_2 islands containing MTBs. (b) Atomically resolved image displaying a single MTB with length $L = 18.0$ nm, indicated by white arrows in (a). (c) Differential conductance color plot extracted from linescan along the red line in (b). (d) Differential conductance spectrum (blue circles) obtained after average between positions marked by red arrows in (c) and the corresponding NRG simulation (red line; $\epsilon = -18.5$ meV, $U = 40.5$ meV, $\gamma = 7.7$ meV). Image information: (a) size 146×108 nm^2, $V_{stab} = 1$ V, $I_{stab} = 11$ pA, $T_s = 0.35$ K; (b) size 20×5 nm^2, $V_{stab} = 100$ mV, $I_{stab} = 10$ pA, $T_s = 0.35$ K; (c) $V_{stab} = 100$ mV, $I_{stab} = 1$ nA, $V_{mod} = 0.5$ mV, $f_{mod} = 719$ Hz, $T_s = 0.35$ K.

freedom, a property of the strong interaction [31,32], applies to the $S = 1/2$ Kondo model, since here, as in the former, the interaction (Kondo exchange) decreases with increasing energy, field, or temperature scales and significantly impacts properties such as the magnetization.

We begin by examining the spin-resolved spectral function of a Kondo system as described by the Anderson impurity model [1,2] (Sec. V in Supplemental Material [33]). An impurity state next to the Fermi level splits into a singly occupied state at ϵ and a doubly occupied state at $\epsilon + U$, owing to the Coulomb repulsion U. The impurity state is exchange coupled to an electron bath, giving rise to the Kondo resonance at the Fermi energy. The hybridization between the impurity and the bath is captured by the width (γ) of the impurity peak. With the three parameters (U, ϵ, γ) at hand, both impurity states and the Kondo resonance can be accessed through simulation within NRG theory (Sec. VI in Supplemental Material [33]). In the absence of an external magnetic field ($B = 0$ T), the spin in the occupied impurity state can freely flip [Fig. 1(a)]. Applying an external field $B > 0$ shifts impurity and Kondo peaks by the Zeeman energy in the spin-averaged spectrum; however, given the higher energy and width of the impurity peaks, the change is only perceptible in the region of the Kondo resonance, causing the latter to split [see Fig. 1(b)]. For the spin-resolved spectral functions, an external field has far-reaching consequences [see Fig. 1(c)]. It shifts almost all the intensity of the up-spin spectral function from the unoccupied peak, far above the Fermi level, to the occupied peak, far below the Fermi level, and the opposite for the down-spin spectral function. Hence, spin-polarized STM should be capable of detecting clear changes in signal intensity in a magnetic field.

The measurements were performed in an ultrahigh vacuum STM operating at $T = 0.35$ K and equipped with a vector magnetic field up to 9 T. Spin-polarized STM tips were prepared by coating a W tip with Fe and checked by imaging the spin spiral on Fe islands on Cu(111) [49] (for details, see Sec. I in Supplemental Material [33]). Fe-coated tips display soft magnetization; i.e., their magnetization follows the direction of the external field. Their spin polarization (p) is in the range of 0.2 to 0.4 [50,51]. The growth of monolayer MoS_2 containing MTBs is achieved on graphene on Ir(111) by Mo deposition in an elemental S pressure of 7×10^{-9} mbar, followed by an annealing to 1050 K in the same S background pressure [52].

The Anderson impurity state is realized as a confined MTB state in an MoS_2 island, which couples to the underlying electron bath of graphene on Ir(111). An MTB is highlighted by white arrows in Fig. 2(a). It exhibits a periodic beating pattern of its confined states close to the Fermi level [Fig. 2(b)]. To establish our Kondo system, it is necessary to have an odd number of electrons in the MTB, achieved when a quantum-confined state resides and splits around the Fermi energy, a condition induced through controlled charging of the MTB via bias pulses [30,53].

To identify the Anderson impurity state, we analyze a series of spin-averaged differential conductance (dI/dV) spectra taken on the MTB, as exemplified in Fig. 2(c), taken along the red line in Fig. 2(b). The inner three peaks comprising the ZBR and the single occupied state below and the doubly occupied state above the Fermi level, in Fig. 2(d) are readily comparable to our spin-averaged NRG simulation (red curve), which uses experimental values for U, ϵ, γ as input.

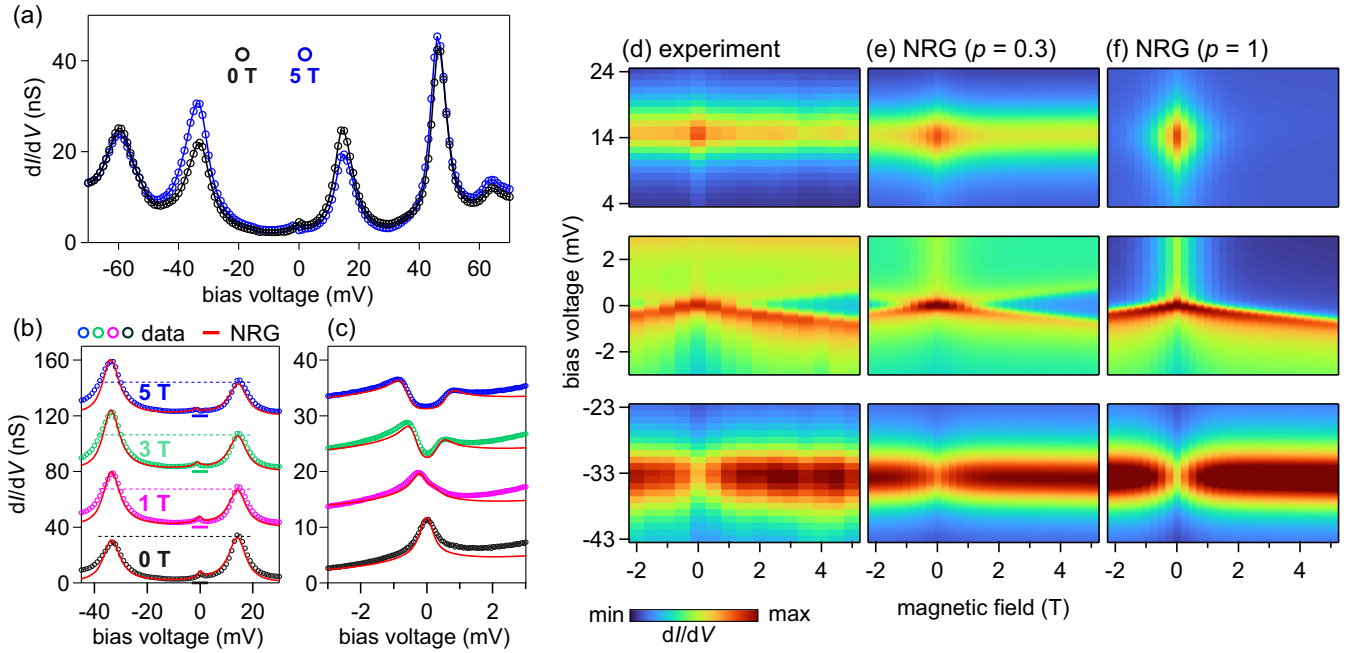

FIG. 3. Spin-polarized STS data of the Kondo effect in MTBs. (a) $\mathrm{d}I/\mathrm{d}V$ spectra with (blue) and without (black) external magnetic field of the impurity peaks and higher order confined states taken with a spin-polarized STM tip. $\mathrm{d}I/\mathrm{d}V$ spectra of the impurity peaks (b) and Kondo resonance (c) at different magnetic fields taken with the same spin-polarized STM tip (colored circles, MTB with $L = 16.6$ nm, $\epsilon = -33.0$ meV, $U = 47.5$ meV, $\gamma = 7.4$ meV) and NRG simulation (red lines) using (1) with a tip polarization of $p = 0.3$. Dashed lines in (b) are a guide to the change in spectral weight. (d)–(f) Differential conductance color plots of the unoccupied impurity peak (top panel), Kondo resonance (middle panel), and occupied impurity peak (bottom panel) as a function of the bias and magnetic field, comparing the experimental $\mathrm{d}I/\mathrm{d}V$ data (d) and NRG simulations with a tip polarization of $p = 0.3$ (e) and $p = 1$ (f). Stabilization parameters: (a),(b) $V_{\mathrm{stab}} = 70$ mV, $I_{\mathrm{stab}} = 1$ nA, $V_{\mathrm{mod}} = 1$ mV, $f_{\mathrm{mod}} = 719$ Hz, $T_{\mathrm{s}} = 0.35$ K; (c) $V_{\mathrm{stab}} = 5$ mV, $I_{\mathrm{stab}} = 1$ nA, $V_{\mathrm{mod}} = 100$ μV, $f_{\mathrm{mod}} = 719$ Hz, $T_{\mathrm{s}} = 0.35$ K.

We now explore how the impurity peaks and the ZBR respond to an external magnetic field using spin-polarized STM. Figure 3(a) shows differential conductance spectra ($\mathrm{d}I/\mathrm{d}V$) at 0 T and under external magnetic field of 5 T normal to the sample surface (spin-polarized measurements of MTB in Fig. 2 shown in Fig. S3 in Supplemental Material [33]). The external field increases the intensity of the occupied impurity peak and the unoccupied peak diminishes, rendering them asymmetric, while the outer, higher energy peaks remain unchanged. The Zeeman effect also leads to a slight change of position of the impurity peaks at 5 T, as compared to 0 T. From the sequences of $\mathrm{d}I/\mathrm{d}V$ spectra at various fields for the impurity peaks [Fig. 3(b)], the continuous change in asymmetry is observed. The field also affects the ZBR [Fig. 3(c)], it is Zeeman split [54] and a spin-excitation steplike increase centered at E_{F} appears. The split ZBRs are also asymmetric in clear correlation with the impurity peaks, i.e., occupied states enhanced and unoccupied states diminished. The field dependence in Figs. 3(b) and 3(c) is due to the spin filter effect caused by the spin-polarized STM tip, since the $\mathrm{d}I/\mathrm{d}V$ signal acquires a dependence on the spin polarization of the tip and the spin-polarized spectral functions of the sample; see Eq. (S9) in [33]. The field-induced changes seen in Fig. 3(a) are not observed with a spin-averaged tip ($p = 0$), as the intensity of impurity peaks is unchanged; see Fig. S2 in [33]. The in-field asymmetry of the impurity states is evidence of the spin-polarized nature of the states and is a direct result of the spectral weight redistribution due to the external field visualized in Fig. 1(c).

To quantify the changes in terms of the spin polarization, we compare our experimental data to field-dependent $\mathrm{d}I/\mathrm{d}V$ spectra simulated within the framework of NRG. At low temperatures, the spin-polarized differential conductance $\mathrm{d}I/\mathrm{d}V$ for the Anderson model is given by (see [33])

$$\frac{\mathrm{d}I}{\mathrm{d}V} \propto [(1+p)/2]\frac{\mathrm{d}I}{\mathrm{d}V_{\uparrow}} + [(1-p)/2]\frac{\mathrm{d}I}{\mathrm{d}V_{\downarrow}}, \qquad (1)$$

where $\mathrm{d}I/\mathrm{d}V_i = (4/\pi\gamma)A_i$, and $A_{i=\uparrow,\downarrow}$ are the energy, temperature, and magnetic-field-dependent spectral functions of the Anderson model, and p is the polarization of the tip. The simulated $\mathrm{d}I/\mathrm{d}V$ is adjusted to match the experimental data at 5 T resulting in an estimated $p = 0.3$, with the simulation displayed as red lines in Figs. 3(b) and 3(c).

With the p obtained for 5 T, all the other fields are simulated with Eq. (1) without further adjustments (constant p), and the NRG-simulated $\mathrm{d}I/\mathrm{d}V$ is displayed

in Figs. 3(b) and 3(c). The simulation resembles the experimental data quite accurately. The agreement is substantiated by comparing the experimental and NRG data color plots for an extended range of magnetic field displayed in Figs. 3(d) and 3(e). In both experiment and theory, the asymmetry between unoccupied (top panels) and occupied (bottom panels) impurity peaks increases as a function of the field and reaches saturation at about 2 T, while the ZBR in the middle panels transforms into a gap with pronounced larger occupied peak at larger fields. The agreement obtained simultaneously for impurity peaks and Kondo resonance with NRG by just introducing a tip spin polarization is unambiguous evidence that the impurity peaks are part of the Kondo system. The effect of a magnetic field on the spin polarization of the MTB can best be visualized by artificially setting $p = 1$, i.e., by assuming that the tip acts as a perfect spin filter. In this case, as shown in Fig. 3(f), only the occupied peak is present at the highest field, while the unoccupied peak is completely suppressed [see also Fig. 1(c)]. Although there is good agreement between the experimental results and NRG, small deviations may arise due to limitations in our model, such as the assumption of a constant g factor, the absence of spin-orbit coupling, and the use of a fixed hybridization function, as further discussed in Sec. VI in [33].

The fact that we can align the magnetic moment using a magnetic field—in analogy to an isolated paramagnetic spin—seems to contradict the Kondo effect, which screens the magnetic moment and thus forms a nonmagnetic spin singlet (at $T = 0$). However, even at $T = 0$, this many-body singlet is polarizable. At finite temperature, information on the polarizability of the Kondo system is contained in the thermodynamic magnetization $m(B,T)$ of the Anderson impurity model describing the MTB (see Sec. VIII in [33]). We can relate the latter to the measured field and temperature dependence of the $\mathrm{d}I/\mathrm{d}V$-weight asymmetry denoted by $A^{w}_{\mathrm{d}I/\mathrm{d}V}$ and defined by

$$A^{w}_{\mathrm{d}I/\mathrm{d}V}(B,T) = \frac{\mathrm{d}I/\mathrm{d}V_a(B,T) - \mathrm{d}I/\mathrm{d}V_b(B,T)}{\mathrm{d}I/\mathrm{d}V_a(B,T) + \mathrm{d}I/\mathrm{d}V_b(B,T)}, \quad (2)$$

where $\mathrm{d}I/\mathrm{d}V_a$ and $\mathrm{d}I/\mathrm{d}V_b$ are the $\mathrm{d}I/\mathrm{d}V$ weights above and below the Fermi level, respectively. Specifically, $m(B,T)$ is related to $A^{w}_{\mathrm{d}I/\mathrm{d}V}(B,T)$ and the spin polarization of the tip (p) via (see [33])

$$m(B,T) = -g\mu_B(A^{w}_{\mathrm{d}I/\mathrm{d}V}(B,T) - A^{w}_{\mathrm{d}I/\mathrm{d}V}(0,T))/2p. \quad (3)$$

Results for the magnetization of MTB obtained in this way, at 0.35 K (blue circles) and at 1.70 K (green circles), are shown in Fig. 4. Also shown are the corresponding magnetizations for the Anderson model within NRG (blue and green solid lines) and for a free spin 1/2 (blue and green dashed lines).

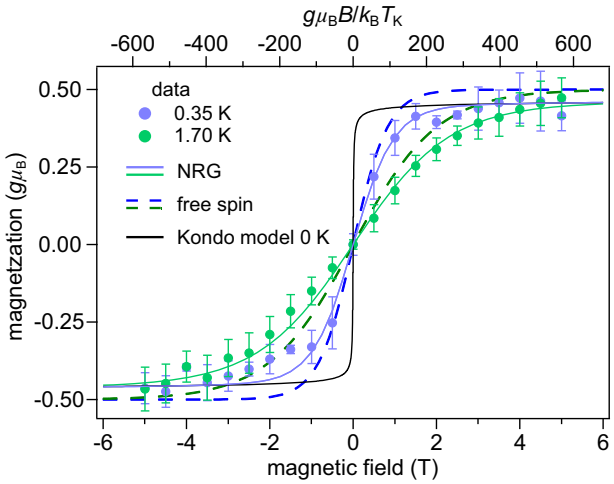

FIG. 4. Field dependence of the magnetization as extracted from the measured asymmetry using (3) for the data in Fig. 3 (blue circles) with $p = 0.3$, and for the data obtained at 1.70 K presented in Fig. S4 of [33] for the same MTB (green circles). Error bars represent the standard deviation of the $A^{w}_{\mathrm{d}I/\mathrm{d}V}(B,T)$ evaluation taken from the different $\mathrm{d}I/\mathrm{d}V$ spectra at impurity maximum locations, following Fig. 2(c). NRG thermodynamic magnetization for the parameters: $\epsilon = -33.0$ meV, $U = 47.5$ meV, $\gamma = 7.4$ meV. Dashed lines: magnetization for a free spin 1/2. Black solid line: $T = 0$ Kondo model magnetization. For a comparable plot featuring a different MTB, see Fig. S5 in [33].

Inspection of Fig. 4 reveals several interesting aspects. First, the experimental data follow the universal magnetization curve of the Anderson model at each temperature. Universality of the magnetization $m(B,T)$ in the Anderson model means that for each fixed T (or equivalently, each fixed T/T_K), $m(B,T)$ is a universal function of $g\mu_B B/k_B T_K$ (whose form changes continuously upon varying T/T_K from 0 to $\gg 1$; see Fig. S12 in [33]). Second, the measured magnetization characterized by a linear increase at low fields only gradually saturates at higher fields. This behavior is in stark contrast to the magnetization curve of a free spin 1/2. The latter saturates rapidly to the fully polarized value $\pm 1/2$ at high fields (dashed lines). The magnetization of the MTB remains lower even at high fields and approaches the fully polarized value only slowly following the NRG magnetization which, for sufficiently high fields, exhibits the theoretically well-known logarithmic corrections. This property of the magnetization is a characteristic of the asymptotic freedom in the Kondo effect [5], resulting in the observed diminished magnetization at high fields. This behavior, most markedly illustrated by the $T = 0$ Kondo model magnetization from the Bethe ansatz [55] (black solid line), is eventually cut off on field scales $g\mu_B B \sim (U\gamma)^{1/2}$ in the case of the Anderson model [7] (for details, see Secs. VIII.A and VIII.B [33]). Above this scale, of order 10–20 meV for our MTBs, the fully polarized (free spin) value would eventually be

restored (Figs. S7 and S8 [33]); however, such large fields (100–200 T) are experimentally inaccessible. The field range used in the experiment is therefore accessing the universal part of the magnetization curve of the Anderson model (see Figs. S7 and S8 in [33]). Finally, the variation of the magnetization with the temperature is also quantitatively well described by the NRG, using just the experimentally measured parameters U, ϵ, and γ.

To conclude, our spin-polarized STM experiments show that the spin-resolved impurity peaks that give rise to a Kondo resonance undergo a massive spectral weight redistribution under external magnetic fields exceeding the thermal energy involved, meaning that the peak below E_F, i.e., occupied state, is composed of majority spin state and the peak at positive bias voltage, i.e., unoccupied state, is dominated by minority spin state. This description is in full agreement with the Anderson model tackled in the framework of NRG. Analysis of the magnetization response of the MTB with respect to field and at different temperatures sheds light on the spin-1/2 character of the system, and reveals the typical signatures of asymptotic freedom characteristic of the Kondo effect, in marked contrast to a free spin 1/2. MTBs provide a versatile realization of the standard model of correlated electrons, the Anderson impurity model, allowing a wide range of Kondo scales to be realized through control of the model parameters U, ϵ, and γ [30]. This, together with spin-polarized STM, opens up new prospects for controllably investigating universal aspects of strongly correlated systems, including investigations of multi-impurity systems [56,57] using MTBs or magnetic MTBs in the presence of superconductivity.

Acknowledgments—We acknowledge funding from Deutsche Forschungsgemeinschaft (DFG) through CRC 1238 (Project No. 277146847, Subprojects No. B06 and No. C02). W. J. acknowledges financial support from the DFG through Project JO 1972/2-1 (Project No. 535290457) within the SPP 2244. T. A. C. gratefully acknowledges computing time on the supercomputer JURECA [58] at Forschungszentrum Jülich under Grant No. JIFF23. J. F. acknowledges financial support from the DFG through project FI 2624/1-1 (Project No. 462692705) within the SPP 2137.

[1] A. C. Hewson, *The Kondo Problem to Heavy Fermions* (Cambridge University Press, Cambridge, England, 1997).
[2] P. W. Anderson, Phys. Rev. **124**, 41 (1961).
[3] K. G. Wilson, Rev. Mod. Phys. **47**, 773 (1975).
[4] H. R. Krishna-murthy, J. W. Wilkins, and K. G. Wilson, Phys. Rev. B **21**, 1003 (1980).
[5] N. Andrei, K. Furuya, and J. H. Lowenstein, Rev. Mod. Phys. **55**, 331 (1983).
[6] N. Kawakami and A. Okiji, Phys. Lett. **86A**, 483 (1981).
[7] P. B. Wiegmann and A. M. Tsvelick, J. Phys. C **16**, 2281 (1983).
[8] J. Li, W.-D. Schneider, R. Berndt, and B. Delley, Phys. Rev. Lett. **80**, 2893 (1998).
[9] V. Madhavan, W. Chen, T. Jamneala, M. F. Crommie, and N. S. Wingreen, Science **280**, 567 (1998).
[10] P. Wahl, L. Diekhöner, G. Wittich, L. Vitali, M. A. Schneider, and K. Kern, Phys. Rev. Lett. **95**, 166601 (2005).
[11] A. Zhao, Q. Li, L. Chen, H. Xiang, W. Wang, S. Pan, B. Wang, X. Xiao, J. Yang, J. G. Hou, and Q. Zhu, Science **309**, 1542 (2005).
[12] A. F. Otte, M. Ternes, K. von Bergmann, S. Loth, H. Brune, C. P. Lutz, C. F. Hirjibehedin, and A. J. Heinrich, Nat. Phys. **4**, 847 (2008).
[13] R. Temirov, A. Lassise, F. B. Anders, and F. S. Tautz, Nanotechnology **19**, 065401 (2008).
[14] S. Trishin, C. Lotze, F. Lohss, G. Franceschi, L. I. Glazman, F. von Oppen, and K. J. Franke, Phys. Rev. Lett. **130**, 176201 (2023).
[15] X. Meng, J. Möller, R. E. Menchón, A. Weismann, D. Sánchez-Portal, A. Garcia-Lekue, R. Herges, and R. Berndt, Nano Lett. **24**, 180 (2024).
[16] M. Ternes, Prog. Surf. Sci. **92**, 83 (2017).
[17] M. Ternes, A. J. Heinrich, and W.-D. Schneider, J. Condens. Matter Phys. **21**, 053001 (2008).
[18] Y.-h. Zhang, S. Kahle, T. Herden, C. Stroh, M. Mayor, U. Schlickum, M. Ternes, P. Wahl, and K. Kern, Nat. Commun. **4**, 2110 (2013).
[19] A. A. Khajetoorians, M. Valentyuk, M. Steinbrecher, T. Schlenk, A. Shick, J. Kolorenc, A. I. Lichtenstein, T. O. Wehling, R. Wiesendanger, and J. Wiebe, Nat. Nanotechnol. **10**, 958 (2015).
[20] S. Mishra, D. Beyer, K. Eimre, S. Kezilebieke, R. Berger, O. Gröning, C. A. Pignedoli, K. Müllen, P. Liljeroth, P. Ruffieux *et al.*, Nat. Nanotechol. **15**, 22 (2020).
[21] J. Li, S. Sanz, J. Castro-Esteban, M. Vilas-Varela, N. Friedrich, T. Frederiksen, D. Peña, and J. I. Pascual, Phys. Rev. Lett. **124**, 177201 (2020).
[22] J. R. Schrieffer and P. A. Wolff, Phys. Rev. **149**, 491 (1966).
[23] W. Hofstetter, Phys. Rev. Lett. **85**, 1508 (2000).
[24] T. A. Costi, Phys. Rev. B **64**, 241310(R) (2001).
[25] Y.-S. Fu, Q.-K. Xue, and R. Wiesendanger, Phys. Rev. Lett. **108**, 087203 (2012).
[26] K. von Bergmann, M. Ternes, S. Loth, C. P. Lutz, and A. J. Heinrich, Phys. Rev. Lett. **114**, 076601 (2015).
[27] D.-J. Choi, S. Guissart, M. Ormaza, N. Bachellier, O. Bengone, P. Simon, and L. Limot, Nano Lett. **16**, 6298 (2016).
[28] T. Frauhammer, H. Chen, T. Balashov, G. Derenbach, S. Klyatskaya, E. Moreno-Pineda, M. Ruben, and W. Wulfhekel, Phys. Rev. Lett. **127**, 123201 (2021).
[29] K. R. Patton, S. Kettemann, A. Zhuravlev, and A. Lichtenstein, Phys. Rev. B **76**, 100408(R) (2007).
[30] C. van Efferen, J. Fischer, T. A. Costi, A. Rosch, T. Michely, and W. Jolie, Nat. Phys. **20**, 82 (2024).
[31] D. J. Gross and F. Wilczek, Phys. Rev. D **8**, 3633 (1973).
[32] H. David Politzer, Phys. Rep. **14**, 129 (1974).

[33] See Supplemental Material at http://link.aps.org/supplemental/10.1103/PhysRevLett.133.246701, which includes Refs. [34–48], for additional experimental data and supporting theory.
[34] S.-H. Phark, J. A. Fischer, M. Corbetta, D. Sander, and J. Kirschner, Appl. Phys. Lett. **103**, 032407 (2013).
[35] D. Sander, S.-H. Phark, M. Corbetta, J. A. Fischer, H. Oka, and J. Kirschner, J. Phys. Condens. Matter **26**, 394008 (2014).
[36] J. Tersoff and D. R. Hamann, Phys. Rev. B **31**, 805 (1985).
[37] A. Schiller and S. Hershfield, Phys. Rev. B **61**, 9036 (2000).
[38] W. Jolie, C. Murray, P. S. Weiß, J. Hall, F. Portner, N. Atodiresei, A. V. Krasheninnikov, C. Busse, H.-P. Komsa, A. Rosch, and T. Michely, Phys. Rev. X **9**, 011055 (2019).
[39] D. E. Logan, M. P. Eastwood, and M. A. Tusch, J. Condens. Matter Phys. **10**, 2673 (1998).
[40] W. C. Oliveira and L. N. Oliveira, Phys. Rev. B **49**, 11986 (1994).
[41] V. L. Campo and L. N. Oliveira, Phys. Rev. B **72**, 104432 (2005).
[42] F. B. Anders and A. Schiller, Phys. Rev. Lett. **95**, 196801 (2005).
[43] R. Peters, T. Pruschke, and F. B. Anders, Phys. Rev. B **74**, 245114 (2006).
[44] A. Weichselbaum and J. von Delft, Phys. Rev. Lett. **99**, 076402 (2007).
[45] R. Bulla, A. C. Hewson, and T. Pruschke, J. Condens. Matter Phys. **10**, 8365 (1998).
[46] F. B. Kugler, Phys. Rev. B **105**, 245132 (2022).
[47] R. Bulla, T. A. Costi, and T. Pruschke, Rev. Mod. Phys. **80**, 395 (2008).
[48] L. Merker, A. Weichselbaum, and T. A. Costi, Phys. Rev. B **86**, 075153 (2012).
[49] S.-H. Phark, J. Fischer, M. Corbetta, D. Sander, K. Nakamura, and J. Kirschner, Nat. Commun. **5**, 5183 (2014).
[50] B. Sinković, E. Shekel, and S. L. Hulbert, Phys. Rev. B **52**, R8696 (1995).
[51] M. Bode, M. Getzlaff, and R. Wiesendanger, Phys. Rev. Lett. **81**, 4256 (1998).
[52] J. Hall, B. Pielić, C. Murray, W. Jolie, T. Wekking, C. Busse, M. Kralj, and T. Michely, 2D Mater. **5**, 025005 (2018).
[53] X. Yang, Z.-L. Gu, H. Wang, J.-J. Xian, S. Meng, N. Nagaosa, W.-H. Zhang, H.-W. Liu, Z.-H. Ling, K. Fan, Z.-M. Zhang, L. Qin, Z.-H. Zhang, Y. Liang, J.-X. Li, and Y.-S. Fu, Natl. Sci. Rev. **10**, nwac210 (2022).
[54] A. Rosch, T. A. Costi, J. Paaske, and P. Wölfle, Phys. Rev. B **68**, 014430 (2003).
[55] N. Andrei, Phys. Lett. **87A**, 299 (1982).
[56] B. A. Jones, C. M. Varma, and J. W. Wilkins, Phys. Rev. Lett. **61**, 125 (1988).
[57] K. Ingersent, A. W. W. Ludwig, and I. Affleck, Phys. Rev. Lett. **95**, 257204 (2005).
[58] Jülich Supercomputing Centre, J. Large-Scale Res. Facil. **7**, A182 (2021).